Research Square

Preprints are preliminary reports that have not undergone peer review.
They should not be considered conclusive, used to inform clinical practice,
or referenced by the media as validated information.

Superconducting Charge Feedback in Semiconductor Nanowires: A Self-Consistent BdG–Poisson Approach

Jinhong Park

jinhongpark@konkuk.ac.kr

Konkuk University

Research Article

Keywords:

Posted Date: November 12th, 2026

DOI: https://doi.org/10.21203/rs.3.rs-11500235/v1

License: This work is licensed under a Creative Commons Attribution 4.0 International License.
Read Full License

Additional Declarations: No competing interests reported.

Superconducting Charge Feedback in Semiconductor Nanowires: A Self-Consistent BdG–Poisson Approach

Jinhong Park[1]

[1] *Department of Physics, Konkuk University, Seoul 05029, Republic of Korea*

(Dated: October 25, 2026)

We develop a computational framework for solving the coupled Bogoliubov–de Gennes and Poisson equations self-consistently in a quasi-one-dimensional geometry and apply it to the gate-induced charge response of a semiconductor nanowire proximity-coupled to a superconductor. Keeping the induced pairing gap fixed, we compare the self-consistent response with a two-step approach that determines the electrostatic potential in the normal state before introducing pairing. Near the semiconductor band edge, the two-step approach substantially underestimates the induced charge under the gate and yields a different spatial profile, even in the linear-response regime. At higher filling, where the Fermi energy greatly exceeds the induced gap, the two approaches closely agree. Calculations of the static density susceptibility connect these contrasting behaviors to pairing-induced changes in the long-wavelength response and the cutoff of the one-dimensional logarithmic enhancement near $2k_F$. Our results demonstrate that superconducting charge feedback must be included in the electrostatic self-consistency to describe the charge response near the semiconductor band edge.

I. INTRODUCTION

Semiconductor–superconductor hybrid devices combine the electrostatic tunability of semiconductors with superconducting pairing induced by the proximity effect. These systems have motivated extensive experimental searches for Majorana zero modes using tunneling and Coulomb-blockade spectroscopy [1–3]. Advances in epitaxial interfaces have enabled semiconductor nanowires with hard induced superconducting gaps [4, 5], while gate-controlled semiconductor weak links have provided a platform for electrically tunable superconducting qubits [6]. Electrostatic gates offer control over carrier occupation and confinement, making the interplay between superconductivity and electrostatics central to understanding and operating these devices.

The electrostatic environment determines more than a shift of the chemical potential. Charge screening, band bending, and the spatial distribution of electronic states influence subband occupation and the coupling between the semiconductor and superconductor. Self-consistent Schrödinger–Poisson calculations have clarified the effects of gates and metallic contacts on nanowire electrostatics [7], the influence of gate voltage and band bending on semiconductor–superconductor hybridization [8, 9], and efficient approaches to treating realistic device geometries [10]. These studies establish the importance of determining the electronic structure together with the electrostatic potential.

Self-consistent treatments of superconducting charge and electrostatics have been used to investigate interaction-induced zero-energy pinning and quantum-dot formation in semiconductor–superconductor nanowires [11]. A frequently employed alternative determines the electrostatic potential self-consistently in the normal state and subsequently introduces superconducting pairing into the electronic Hamiltonian [7, 8]. This two-step approach incorporates normal-state charge screening but omits the feedback of the pairing-induced charge redistribution onto the electrostatic potential. Its omission is motivated by the weak influence of pairing on electrostatics when the relevant Fermi energy greatly exceeds the superconducting gap. Near a semiconductor band edge, however, this separation of energy scales is lost, raising the question of whether normal-state electrostatics remains sufficient to describe the superconducting charge response.

In this work, we develop a computational framework for solving the coupled Poisson and Bogoliubov–de Gennes (BdG) equations self-consistently in a quasi-one-dimensional superconducting wire. The framework incorporates the superconducting charge density into the electrostatic calculation while treating the induced pairing gap as a fixed parameter. As an application, we investigate the charge response of a proximitized semiconductor nanowire to a local gate potential. We compare the fully self-consistent response with a two-step calculation, in which the electrostatic potential is determined in the normal state and subsequently used to calculate the superconducting density without further electrostatic feedback.

Our calculations reveal distinct behaviors depending on the reference Fermi energy relative to the induced superconducting gap. At sufficiently high filling, superconducting charge feedback produces only a small correction to the two-step result. Near the band edge, however, it substantially modifies both the spatial distribution and the integrated magnitude of the gate-induced charge. This difference persists in the linear-response regime. We interpret these contrasting behaviors through the static density susceptibility and its role in electrostatic screening. These results demonstrate that determining the potential in the normal state and subsequently introducing superconductivity fails to capture the gate-induced charge response, particularly near the band edge. A self-consistent treatment of superconducting charge feedback is therefore essential in this regime.

Throughout this paper, the electron charge is denoted by $-e$, with $e > 0$.

II. SELF-CONSISTENT BDG-POISSON APPROACH

We consider a proximitized semiconductor wire subject to a local electrostatic gate, as illustrated in Fig. 1(a). The wire lies at $z = 0$, and a finite gate electrode is positioned above its central region. Electronic motion is restricted to the wire direction, while the electrostatic potential is calculated in the surrounding two-dimensional (x, z) domain. A reservoir tunnel-coupled to the wire fixes its equilibrium electrochemical potential ξ, whereas the local chemical potential satisfies $\mu(x) = \xi + e\phi(x)$, where $\phi(x) \equiv \phi(x, z = 0)$.

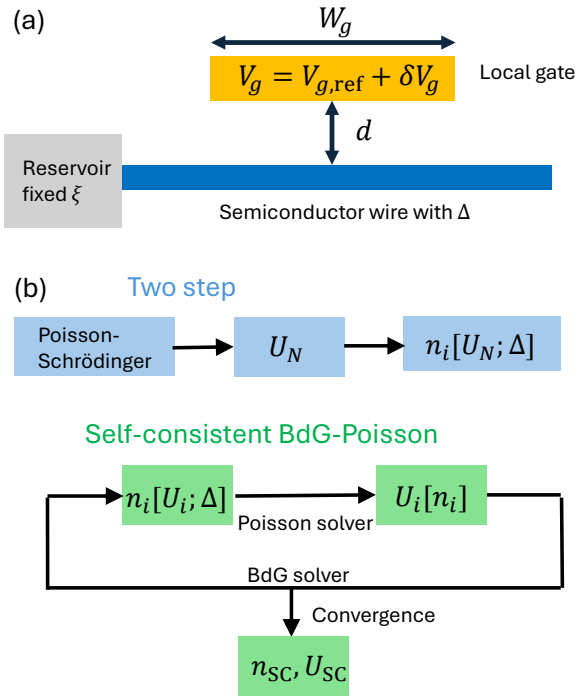


Figure 1. Schematic setup and computational approaches. (a) A proximitized semiconductor wire with a fixed induced pairing gap Δ is coupled to a reservoir at electrochemical potential ξ. A local gate of width W_g is separated from the wire by a distance d. Its voltage is $V_g = V_{g,\mathrm{ref}} + \delta V_g$, where the reference satisfies $\mu_{\mathrm{ref}} - eV_{g,\mathrm{ref}} = \xi$, with $e > 0$. (b) In the two-step approach, a self-consistent normal-state Poisson–Schrödinger calculation determines the potential U_N, which is subsequently held fixed when evaluating the superconducting density. In the self-consistent BdG–Poisson approach, the superconducting density and electrostatic potential are updated iteratively until convergence, yielding n_{SC} and U_{SC}. The pairing gap is held fixed in both approaches.

To compare different fillings, we introduce a normal-state reference characterized by the chemical potential μ_{ref} and the corresponding uniform density n_{ref}. Its reference gate voltage satisfies

$$\mu_{\mathrm{ref}} - eV_{g,\mathrm{ref}} = \xi. \tag{1}$$

The local gate perturbation is measured by $\delta V_g = V_g - V_{g,\mathrm{ref}}$. We discretize the wire into N sites at positions x_i, with lattice spacing a. The electronic potential energy at site i, measured relative to the reference, is then

$$U_i = -e[\phi(x_i, 0) - V_{g,\mathrm{ref}}], \tag{2}$$

such that the local chemical potential is $\mu_i = \mu_{\mathrm{ref}} - U_i$. Thus, changing μ_{ref} at fixed ξ entails a corresponding shift of the reference gate voltage. Experimentally, the reference filling can be controlled by a global back gate, not shown in Fig. 1(a). Here, its effect is represented by the reference parameters μ_{ref} and n_{ref}, without explicitly including the back gate in the electrostatic geometry.

The equilibrium density and electrostatic potential energy must be determined together. For a given potential-energy profile $\{U_i\}$, the BdG Hamiltonian determines the electronic density $\{n_i\}$, which in turn acts as the charge source for Poisson's equation and modifies $\{U_i\}$. A self-consistent solution thus requires $\{n_i\}$ and $\{U_i\}$ to satisfy both equations simultaneously, as illustrated by the self-consistent BdG–Poisson loop shown in green in Fig. 1(b).

We describe the electrostatic part first. We solve Poisson's equation in the (x, z) domain using a finite-element method, imposing the gate potential as a Dirichlet boundary condition. The excess wire density relative to n_{ref} enters through the electric-field boundary condition at the wire boundary $z = 0$ [Fig. 1(a)]. Specifically, we impose

$$\hat{\boldsymbol{n}} \cdot \nabla\phi|_{(x_i,0)} = -C\,(n_i - n_{\mathrm{ref}})\,, \tag{3}$$

where $\hat{\boldsymbol{n}}$ is the outward unit normal of the electrostatic domain, and the boundary source between neighboring wire sites is obtained by linear interpolation. The positive coefficient C sets the electrostatic coupling strength and has units of voltage per unit length. On all remaining outer boundaries, we impose a vanishing normal electric field.

In the absence of excess wire charge, i.e., $n(x) = n_{\mathrm{ref}}$, these boundary conditions admit the uniform solution $\phi(x, z) = V_g$. The corresponding potential energy relative to the reference is thus $-e(V_g - V_{g,\mathrm{ref}}) \equiv -e\delta V_g$. Including the excess charge, linearity of Poisson's equation gives

$$U_i = -e\delta V_g + \sum_j \mathcal{K}_{ij}(n_j - n_{\mathrm{ref}})\,. \tag{4}$$

Here, $\mathcal{K}_{ij}$ is the electrostatic response matrix obtained from the finite-element solution [10]. To construct its jth column, we apply a discrete unit excess-density profile $n_k - n_{\mathrm{ref}} = \delta_{kj}$ at zero gate perturbation, $\delta V_g = 0$. The source profile is linearly interpolated along the wire boundary, and the resulting potential energy at site i defines $\mathcal{K}_{ij}$.

Once $\mathcal{K}_{ij}$ is determined, the potential energy U_i for a given electronic density profile is evaluated using Eq. (4), without solving the finite-element Poisson problem again. Before evaluating this expression, we smooth the input density using a Gaussian kernel with standard deviation $2a$ and use the resulting values for n_j.

We next calculate the electronic density for the potential-energy profile $\{U_i\}$ obtained from the Poisson solver through Eq. (4). We consider the simplest case of a spin-degenerate wire with a uniform induced s-wave pairing gap Δ. The mean-field Hamiltonian is

$$\hat{H} = \sum_{ij,\sigma} h_{ij}\hat{c}^\dagger_{i\sigma}\hat{c}_{j\sigma} + \sum_i \left(\Delta\hat{c}^\dagger_{i\uparrow}\hat{c}^\dagger_{i\downarrow} + \text{H.c.}\right), \tag{5}$$

$$h_{ij} = (2t - \mu_{\text{ref}} + U_i)\delta_{ij} - t(\delta_{i,j+1} + \delta_{i,j-1}), \tag{6}$$

where $\hat{c}_{i\sigma}$ annihilates an electron with spin σ at site i, and $t = \hbar^2/(2m^*a^2)$ is the hopping amplitude for effective mass m^*. We use periodic boundary conditions along the wire and choose Δ to be real.

We compute the superconducting density by first diagonalizing the normal-state single-particle Hamiltonian h_{ij} in Eq. (6),

$$\sum_j h_{ij}\psi_\nu(j) = E_\nu\psi_\nu(i), \tag{7}$$

where the corresponding positive BdG quasiparticle energies are $\mathcal{E}_\nu = \sqrt{E_\nu^2 + \Delta^2}$. Then, the spin-summed local density is given by

$$n_i = \sum_\nu |\psi_\nu(i)|^2 \left[1 - \frac{E_\nu}{\mathcal{E}_\nu}\tanh\left(\frac{\mathcal{E}_\nu}{2k_BT}\right)\right]. \tag{8}$$

The Poisson relation and the BdG density expression together define the coupled self-consistent problem. Starting from a trial potential, we evaluate the electronic density and use it to obtain a new potential from Eq. (4). Repeating these steps yields the equilibrium density n_i and potential U_i, as illustrated in green in Fig. 1(b).

To reduce the computational cost of preparing an initial potential, we first solve the coupled problem within a local-density approximation (LDA). At each site, the density is approximated by that of a uniform wire with chemical potential $\mu_i = \mu_{\text{ref}} - U_i$,

$$n_i^{\text{LDA}} = \frac{1}{N}\sum_k \left[1 - \frac{\varepsilon_{ki}}{\mathcal{E}_{ki}}\tanh\left(\frac{\mathcal{E}_{ki}}{2k_BT}\right)\right], \tag{9}$$

where $\varepsilon_{ki} = 2t[1 - \cos(ka)] - \mu_{\text{ref}} + U_i$ and $\mathcal{E}_{ki} = \sqrt{\varepsilon_{ki}^2 + \Delta^2}$. The sum runs over the momenta of the periodic wire. This approximation avoids repeated diagonalization during the initial electrostatic adjustment, while retaining the full nonlocal Poisson response. The resulting potential profile serves as the initial condition for the subsequent self-consistent iteration using the eigenstate-based density.

Using the resulting LDA potential as the initial condition, we iterate and solve the self-consistent BdG-Poisson equations. To stabilize these iterations, the potential is updated by linear mixing,

$$U_i^{(m+1)} = U_i^{(m)} + \eta\left[U_i^{\text{P}}[n^{(m)}] - U_i^{(m)}\right], \tag{10}$$

where $U_i^{\text{P}}[n^{(m)}]$ is the Poisson potential obtained from the density at iteration m, and η is the mixing parameter, chosen between 0.001 and 0.002. The iteration is repeated until the unmixed potential residual satisfies $\max_i \left|U_i^{\text{P}}[n^{(m)}] - U_i^{(m)}\right| < 10^{-6}\,\text{meV}$, and the change in total electron number satisfies $\left|\sum_i n_i^{(m)} - \sum_i n_i^{(m-1)}\right| < 10^{-7}$.

For comparison, we also perform a two-step calculation in which the electrostatic potential is determined before superconducting pairing is introduced, following the strategy employed in Refs. [7, 8]. We first solve the coupled density–Poisson problem at $\Delta = 0$, obtaining the normal-state potential U_N and density n_N. Keeping U_N fixed, we then evaluate the superconducting density $n_{\text{two}} = n[U_N; \Delta]$, as illustrated by the blue boxes in Fig. 1(b). In contrast, the self-consistent BdG–Poisson calculation yields $n_{\text{SC}} = n[U_{\text{SC}}; \Delta]$, with the superconducting density included in the determination of U_{SC}. In the next section, we study the gate-induced charge response to demonstrate why including superconducting electrostatic feedback is essential near the semiconductor band edge.

III. GATE-INDUCED CHARGE RESPONSE

We apply the framework developed in Sec. II to study the density response induced by a gate voltage and compare the normal-state, two-step, and self-consistent superconducting responses. For each calculation, we define the gate-induced density change relative to its own reference state at $\delta V_g = 0$,

$$\delta n_{\alpha,i} = n_{\alpha,i}(\delta V_g) - n_{\alpha,i}(0), \tag{11}$$

where $\alpha = N, \text{two}, \text{SC}$. Subtracting the corresponding reference separates the response to the local gate from the density redistribution already present when superconductivity is introduced. We vary the reference filling while keeping the induced gap, electrostatic geometry, and relative gate voltage δV_g fixed.

Figure 2 compares the density responses at three reference fillings. At $\mu_{\text{ref}}/\Delta = 0.3$ [Fig. 2(a)], introducing superconductivity substantially reduces the gate-induced density relative to the normal-state result (blue dashed line). However, the magnitude of this reduction depends strongly on whether electrostatic feedback is included. The two-step calculation (orange dotted line) predicts a considerably smaller response than the self-consistent BdG–Poisson calculation (green solid line). Including electrostatic feedback partially compensates the superconductivity-induced suppression of the gate response, so that the self-consistent response lies between the normal-state and two-step results.

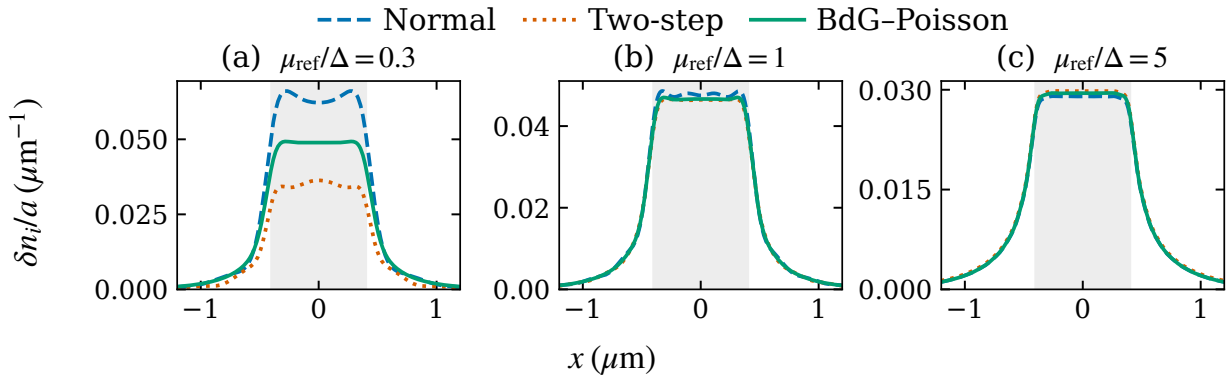


Figure 2. Gate-induced density response of a proximitized semiconductor nanowire for (a) $\mu_{\rm ref}/\Delta = 0.3$, (b) 1, and (c) 5. The curves compare the self-consistent normal-state calculation (blue dashed), the two-step superconducting calculation with the normal-state electrostatic potential held fixed (orange dotted), and the self-consistent BdG–Poisson calculation (green solid). For each method $\alpha = N, \text{two}, \text{SC}$, we plot $\delta n_{\alpha,i}/a$ as a function of the site position x_i, where $\delta n_{\alpha,i} = n_{\alpha,i}(\delta V_g) - n_{\alpha,i}(0)$ and $\delta V_g = V_g - V_{g,\rm ref}$. The reference gate voltage satisfies $\mu_{\rm ref} - eV_{g,\rm ref} = \xi$, where ξ is the fixed reservoir electrochemical potential and $e > 0$. The shaded region indicates the local gate of width $0.8\,\mu$m. Parameters are $N = 1280$, $a = 10\,$nm, $t = 15.24\,$meV, $d = 50\,$nm, $eaC = 1\,$meV, $\Delta = 0.2\,$meV, $k_BT = 0.01\,$meV, and $e\delta V_g = 0.005\,$meV.

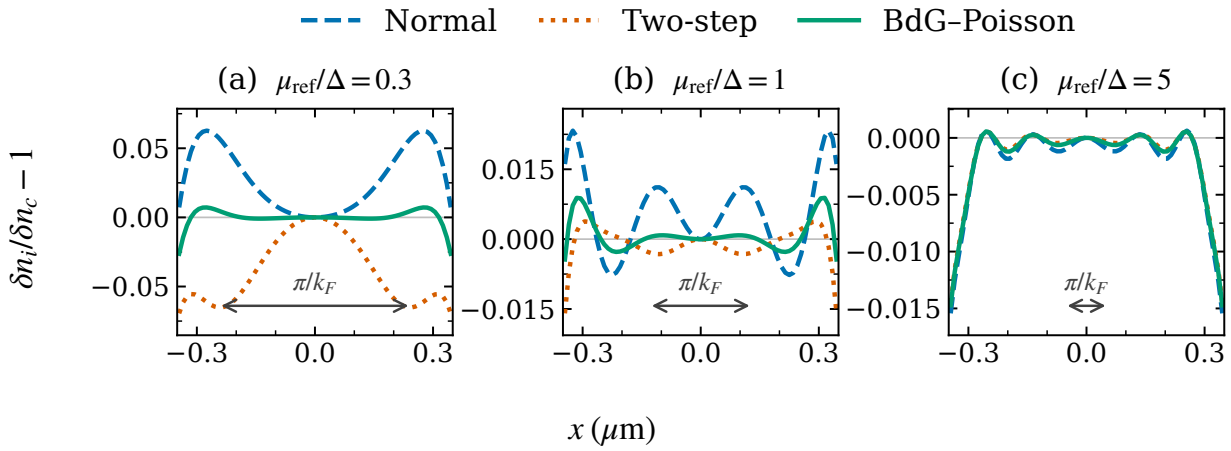


Figure 3. Normalized density response near the gate center for (a) $\mu_{\rm ref}/\Delta = 0.3$, (b) 1, and (c) 5. Each response is normalized by its own central value, showing $\delta n_{\alpha,i}/\delta n_{\alpha,c} - 1$ with $\alpha = N, \text{two}, \text{SC}$, where $\delta n_{\alpha,c}$ is obtained by linear interpolation of the site responses at $x = 0$. Colors and line styles follow Fig. 2. The arrows indicate the reference $2k_F$ oscillation period π/k_F, with $2t[1 - \cos(k_F a)] = \mu_{\rm ref}$. Different vertical scales are used in the three panels for clarity. All parameters are the same as in Fig. 2.

The discrepancy decreases markedly as the reference filling increases. At $\mu_{\rm ref}/\Delta = 1$ [Fig. 2(b)], the two superconducting responses nearly coincide, although both remain slightly below the normal-state response. At $\mu_{\rm ref}/\Delta = 5$ [Fig. 2(c)], all three responses are close. Thus, the two-step approach captures the response magnitude at higher filling but misses an appreciable contribution from superconducting electrostatic feedback near the band edge.

To quantify this difference, we evaluate the excess electron number beneath the gate,

$$\delta N_{\alpha,\rm gate} = \sum_{i:\,|x_i| \le W_g/2} \delta n_{\alpha,i}. \tag{12}$$

At $\mu_{\rm ref}/\Delta = 0.3$, the two-step result is approximately 29% smaller than the self-consistent result. Halving δV_g changes $\delta N_{\alpha,\rm gate}/\delta V_g$ by less than 0.4% for all three calculations, while leaving the relative discrepancy between the two-step and self-consistent results nearly unchanged. The discrepancy thus persists in the linear-response regime.

Figure 3 resolves the spatial variation near the gate center by plotting $\delta n_{\alpha,i}/\delta n_{\alpha,c} - 1$. At $\mu_{\rm ref}/\Delta = 0.3$

[Fig. 3(a)], the normal-state response exhibits a central minimum with two neighboring maxima, whereas the two-step response shows the opposite structure, with a central maximum and neighboring minima. The self-consistent BdG–Poisson response is considerably flatter in the central region. At $\mu_{\rm ref}/\Delta = 1$ [Fig. 3(b)], the normal-state response displays several oscillations, while both superconducting responses show smaller spatial variations. At $\mu_{\rm ref}/\Delta = 5$ [Fig. 3(c)], weak oscillations remain in all three responses, and the two-step and self-consistent superconducting profiles nearly coincide. The oscillation spacing decreases with increasing filling and is consistent with the reference period π/k_F indicated by the arrows.

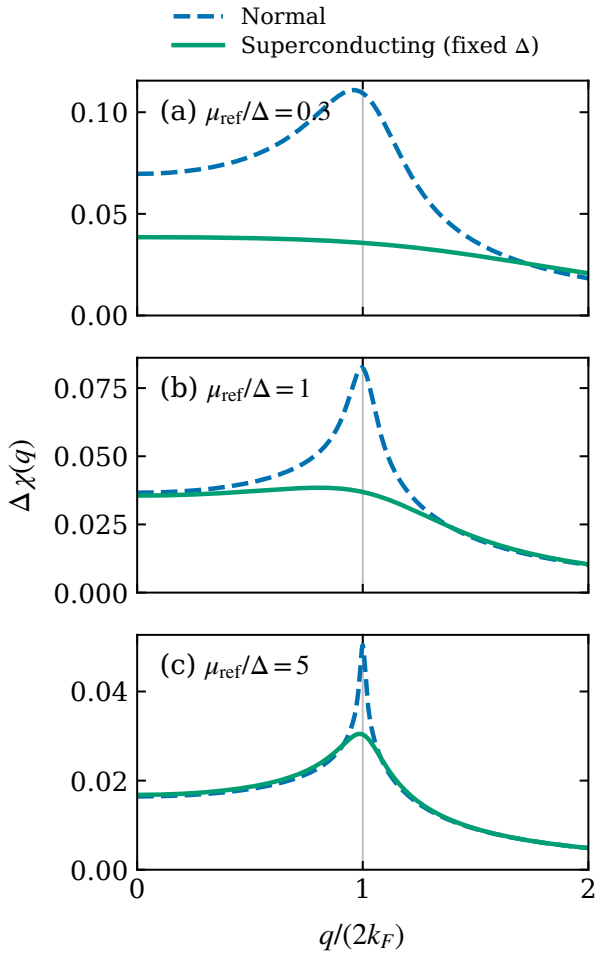


Figure 4. Static density susceptibility of a uniform wire for (a) $\mu_{\rm ref}/\Delta = 0.3$, (b) 1, and (c) 5. The blue dashed and green solid curves show the normal-state susceptibility $\chi_N(q)$ and the superconducting susceptibility $\chi_{\rm SC}(q)$ at fixed pairing gap, respectively, before electrostatic feedback is included. The vertical lines mark $q = 2k_F$, where $2t[1-\cos(k_F a)] = \mu_{\rm ref}$. Parameters are $\Delta = 0.2\,$meV for the superconducting calculation and $k_B T = 0.01\,$meV for both calculations. The normal-state calculation uses zero pairing. The vertical axis shows $\Delta\chi_\alpha(q)$, with $\chi_\alpha(q)$ defined per lattice site.

These oscillations originate from the $2k_F$ component of the one-dimensional density. Decomposing the electron field near the two Fermi points as $\hat{\psi}_\sigma(x) \simeq e^{ik_F x}\hat{R}_\sigma(x) + e^{-ik_F x}\hat{L}_\sigma(x)$, the density contains the contribution

$$\hat{n}_{2k_F}(x) = \sum_\sigma \left[e^{-2ik_F x}\hat{R}^\dagger_\sigma(x)\hat{L}_\sigma(x) + \text{H.c.} \right], \qquad (13)$$

where $\hat{R}_\sigma$ and $\hat{L}_\sigma$ denote slowly varying right- and left-moving fields, respectively. This term connects right- and left-moving states and describes the density response associated with backscattering [12].

To understand how superconducting pairing modifies these spatial profiles, we calculate the static density susceptibilities $\chi_N(q)$ and $\chi_{\rm SC}(q)$ of a uniform wire before including electrostatic feedback. They are defined through $\delta n_\alpha(q) = -\chi_\alpha(q)\delta U(q)$, where $\delta n_\alpha(q)$ is the Fourier component of $\delta n_{\alpha,i}$, with $\alpha = N, {\rm SC}$ and the pairing gap held fixed in the superconducting calculation. The occupation per spin in the superconducting state is obtained from Eq. (8), given by

$$f_{k,{\rm SC}} = \frac{1}{2}\left[1 - \frac{\epsilon_k}{\mathcal{E}_k}\tanh\left(\frac{\mathcal{E}_k}{2k_B T}\right)\right], \qquad (14)$$

where $\epsilon_k = 2t[1-\cos(ka)] - \mu_{\rm ref}$ and $\mathcal{E}_k = \sqrt{\epsilon_k^2 + \Delta^2}$ are the uniform-wire energies obtained by setting $U_i = 0$. In the normal state, this reduces to the Fermi–Dirac distribution, $f_{k,N} = f(\epsilon_k)$. Linearizing Eq. (8) with respect to a static potential modulation yields

$$\chi_\alpha(q) = \frac{2}{N_k}\sum_k \frac{f_{k,\alpha} - f_{k+q,\alpha}}{\epsilon_{k+q} - \epsilon_k}, \qquad \alpha = N, {\rm SC}\,. \qquad (15)$$

Here, N_k is the number of momentum points used in the sum, and the factor of two accounts for spin degeneracy.

Figure 4 compares the normal and superconducting susceptibilities at the three reference fillings. The normal-state response exhibits an enhancement near $q = 2k_F$, associated with the well-known logarithmic singularity of the one-dimensional static susceptibility at zero temperature [12]. The finite temperature rounds this singularity. Although the temperature is fixed, increasing the reference filling reduces $k_B T/\mu_{\rm ref}$, making the normal-state peak narrower on the scaled momentum axis $q/(2k_F)$.

Superconducting pairing rounds and suppresses this enhancement by smoothing the occupation $f_{k,{\rm SC}}$ over an energy range of order Δ, thereby cutting off the logarithmic singularity even at zero temperature. At higher filling, $\mu_{\rm ref} \gg \Delta$, the affected momenta remain close to the Fermi points, and a maximum near $2k_F$ survives with a substantially reduced height [Fig. 4(c)]. As $\mu_{\rm ref}$ decreases to Δ, the momentum range broadens relative to k_F, producing a less pronounced maximum [Fig. 4(b)]. At still lower filling, the redistribution is no longer confined near the Fermi points, and the distinct $2k_F$ feature is washed out [Fig. 4(a)].

Pairing also substantially suppresses the long-wavelength susceptibility $\chi_{\rm SC}(0) = \partial n_i/\partial\mu_{\rm ref}|_\Delta$ near the band edge, whereas its normal-state value is nearly recovered at higher filling. This change in the long-wavelength response complements the suppression of the $2k_F$ feature and helps explain the filling dependence of the gate-response magnitude in Fig. 2.

These susceptibility results provide a physical interpretation of the charge responses near the band edge. Pairing modifies both the long-wavelength response and the $2k_F$ structure, affecting the magnitude and spatial variation of the induced density. The two-step approach includes these changes only in the final density evaluation, while retaining the electrostatic potential determined by normal-state screening. The self-consistent BdG–Poisson approach also incorporates the modified density into the screening process. This additional feedback accounts for the substantial difference between the two approaches at low filling and establishes the importance of superconducting electrostatic self-consistency near the band edge of a semiconductor wire proximity-coupled to a superconductor.

IV. CONCLUSION AND OUTLOOK

We have developed a self-consistent BdG–Poisson framework and applied it to the gate-induced charge response of a semiconductor wire proximity-coupled to a superconductor. Near the band edge, superconducting pairing modifies both the long-wavelength density susceptibility and its $2k_F$ structure, making superconducting charge feedback essential for describing the magnitude and spatial profile of the response. Consequently, determining the electrostatic potential in the normal state and subsequently introducing pairing fails to capture the charge response in this regime, even within linear response. At higher filling, the two-step and self-consistent results become closely aligned. These findings identify the semiconductor band-edge regime as a setting where superconductivity must be included in the electrostatic self-consistency, even when the induced pairing gap is fixed.

The framework can be extended to semiconductor nanowires with spin–orbit coupling and Zeeman splitting by evaluating the charge density from the full BdG Hamiltonian. Since tuning the chemical potential near a subband edge is relevant to accessing regimes that support Majorana zero modes, superconducting charge feedback may also affect the gate response and electrostatic profiles of these devices. The present framework provides a basis for examining these effects beyond normal-state electrostatics.

ACKNOWLEDGMENTS

This work was supported by Konkuk University in 2025 (Grant No. 2025-A019-0020).

[1] V. Mourik, K. Zuo, S. M. Frolov, S. R. Plissard, E. P. A. M. Bakkers, and L. P. Kouwenhoven, Signatures of Majorana fermions in hybrid superconductor-semiconductor nanowire devices, Science **336**, 1003 (2012).
[2] A. Das, Y. Ronen, Y. Most, Y. Oreg, M. Heiblum, and H. Shtrikman, Zero-bias peaks and splitting in an Al–InAs nanowire topological superconductor as a signature of Majorana fermions, Nature Physics **8**, 887 (2012).
[3] S. M. Albrecht, A. P. Higginbotham, M. H. Madsen, F. Kuemmeth, T. S. Jespersen, J. Nygård, P. Krogstrup, and C. M. Marcus, Exponential protection of zero modes in Majorana islands, Nature **531**, 206 (2016).
[4] P. Krogstrup, N. L. B. Ziino, W. Chang, S. M. Albrecht, M. H. Madsen, E. Johnson, J. Nygård, C. M. Marcus, and T. S. Jespersen, Epitaxy of semiconductor–superconductor nanowires, Nature Materials **14**, 400 (2015).
[5] W. Chang, S. M. Albrecht, T. S. Jespersen, F. Kuemmeth, P. Krogstrup, J. Nygård, and C. M. Marcus, Hard gap in epitaxial semiconductor–superconductor nanowires, Nature Nanotechnology **10**, 232 (2015).
[6] T. W. Larsen, K. D. Petersson, F. Kuemmeth, T. S. Jespersen, P. Krogstrup, J. Nygård, and C. M. Marcus, Semiconductor-nanowire-based superconducting qubit, Physical Review Letters **115**, 127001 (2015).
[7] A. Vuik, D. Eeltink, A. R. Akhmerov, and M. Wimmer, Effects of the electrostatic environment on the Majorana nanowire devices, New Journal of Physics **18**, 033013 (2016).
[8] A. E. Antipov, A. Bargerbos, G. W. Winkler, B. Bauer, E. Rossi, and R. M. Lutchyn, Effects of gate-induced electric fields on semiconductor Majorana nanowires, Physical Review X **8**, 031041 (2018).
[9] A. E. G. Mikkelsen, P. Kotetes, P. Krogstrup, and K. Flensberg, Hybridization at superconductor-semiconductor interfaces, Physical Review X **8**, 031040 (2018).
[10] B. D. Woods, T. D. Stanescu, and S. Das Sarma, Effective theory approach to the Schrödinger-Poisson problem in semiconductor Majorana devices, Physical Review B **98**, 035428 (2018).
[11] S. D. Escribano, A. Levy Yeyati, and E. Prada, Interaction-induced zero-energy pinning and quantum dot formation in Majorana nanowires, Beilstein Journal of Nanotechnology **9**, 2171 (2018).
[12] T. Giamarchi, *Quantum Physics in One Dimension* (Oxford University Press, Oxford, 2004).